

Metallo-cyclic Receptors with Re^I/Os^{II}-Based Moieties: Molecular Photophysics and Selective Molecular Sensing

Dengfeng Xu, Kay T. Khin, Wytze E. van der Veer, Joseph W. Ziller, and Bo Hong*^[a]

Abstract: New metallo-cyclic Re^I and Os^{II} complexes with polyphosphane/poly-yne spacers, including dimers $[\{\text{Re}(\text{CO})_3\text{Cl}(\text{C}_{2n}\text{P}_2)\}_2]$ ($n = 1, \mathbf{1}; 2, \mathbf{2}$) and tetramers $[\{\text{Re}(\text{CO})_3\text{Cl}(\text{C}_{2n}\text{P}_2)\}_4]$ ($n = 1, \mathbf{3}; 2, \mathbf{4}$, $\text{C}_2\text{P}_2 = \text{Ph}_2\text{P}-\text{C}\equiv\text{C}-\text{PPh}_2$, $\text{C}_4\text{P}_2 = \text{Ph}_2\text{P}-\text{C}\equiv\text{C}-\text{C}\equiv\text{C}-\text{PPh}_2$), as well as the mixed-metal $[\{\text{Re}(\text{CO})_3\text{Cl}\}_2\{\text{Os}(\text{bpy})_2\}_2(\text{C}_2\text{P}_2)_4](\text{PF}_6)_4$ ($\mathbf{6}$, $\text{bpy} = 2,2'$ -bipyridine) and its precursor $[\text{Os}(\text{bpy})_2(\text{C}_2\text{P}_2)_2](\text{PF}_6)_2$ ($\mathbf{5}$) have been synthesized. Characterization has been carried out using $^{31}\text{P}\{^1\text{H}\}$ NMR, FAB/MS, ESI/MS, IR spectroscopy, elemental analysis (EA), and X-ray single crystal structure determination. These new

metallo-cyclic complexes are found to be emissive, with a characteristic Re^I-based emission at 505–525 nm (lifetimes of 3.4–6.8 ns) and an Os^{II}-based emission at 600–605 nm (lifetimes of 650–675 ns). High quantum yields of 0.25 and 0.17 were observed for $\mathbf{5}$ and $\mathbf{6}$, which were representative of the few most emissive species reported with Os^{II} centers. Efficient energy transfer from the Re^I donor to the Os^{II} acceptor was

also found. In addition, a host–guest study was performed using emissive metallo-cyclic $\mathbf{6}$, and host–guest binding constants of 775M^{-1} , 1580M^{-1} , and 1680M^{-1} were obtained for the guests anisole, 1,4-dimethoxybenzene, and 1,3,5-trimethoxybenzene, respectively. The correlation between the guest molecule size, cavity dimension, and the host–guest binding constant is discussed. Furthermore, the relationship between the π -acceptor ability of the nonchromophoric phosphanes, the energy gap between the ground and excited state, and the nonradiative decay rate constant (k_{nr}) is also explored.

Keywords: host–guest systems • macrocycles • osmium • photoluminescence • rhenium

Introduction

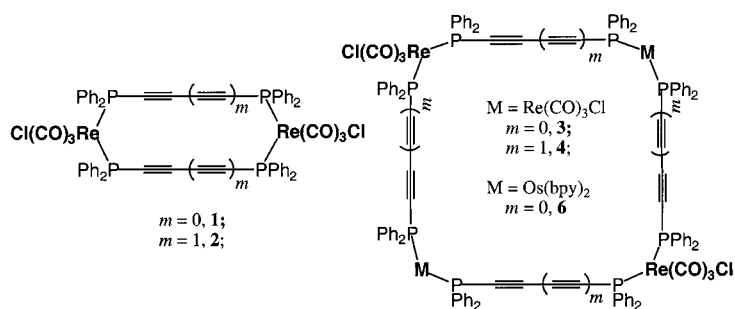
The construction and study of well-defined metal-containing macrocyclic molecular systems (metallo-cyclic receptors or inorganic cyclophanes) constitute one of the current research areas in modern supramolecular chemistry.^[1–7] Recent interest in this area has intensified due to the multifaceted characteristics of these metallo-cycles, including versatile structural features and various desirable functional properties such as redox activity,^[2d, 4a] photoluminescence,^[1d, 3, 4, 6, 7] chirality,^[1e] and magnetism.^[2f] With a judicious choice of metal-based moieties and rigid spacers, the distance between metal centers and the cavity size can be controlled and fine-tuned. As a result, it is then possible to probe the selective molecular sensing and host–guest chemistry using metallo-cycles as hosts or receptors and organic guest molecules with various sizes.^[5] The degree of electronic communication and redox interaction between metal centers can also be studied, and furthermore, with suitable combinations of donor/acceptor pairs, the

efficiency and rate constant of intramolecular electron/energy transfer within macrocyclic platforms can be investigated.

We have recently become interested in the design and study of metallo-cyclic species that contain ditopic phosphane spacers with sp carbon chains and various photo- and redox-active metal-based moieties. Using Ru^{II}(tpy)-based dimeric and trimeric macrocycles with a $\text{Ph}_2\text{P}-\text{C}\equiv\text{C}-\text{C}\equiv\text{C}-\text{PPh}_2$ (C_4P_2) spacer^[4a] and Pd^{II}/Pt^{II} macrocyclic dimers with $\text{Ph}_2\text{P}-\text{C}\equiv\text{C}-\text{PPh}_2$ (C_2P_2),^[4b] we have studied the dual capability of these systems in molecular recognition through host–guest interactions and electronic communication between multiple redox centers within a macrocyclic platform. As a relatively new type of spacer unit, polyphosphane/poly-yne spacers such as C_2P_2 and C_4P_2 provide important rigidity and structural control of cavity sizes in our new macrocyclic complexes.

In this paper, we report the synthesis, purification, and characterization of new metallo-cyclic species with Re^I and Os^{II} centers, including the dimeric $[\{\text{Re}(\text{CO})_3\text{Cl}(\text{C}_{2n}\text{P}_2)\}_2]$ ($n = 1, \mathbf{1}; n = 2, \mathbf{2}$), tetrameric $[\{\text{Re}(\text{CO})_3\text{Cl}(\text{C}_{2n}\text{P}_2)\}_4]$ ($n = 1, \mathbf{3}; n = 2, \mathbf{4}$), and the mixed-metal species $[\{\text{Re}(\text{CO})_3\text{Cl}\}_2\{\text{Os}(\text{bpy})_2\}_2(\text{C}_2\text{P}_2)_4](\text{PF}_6)_4$ ($\mathbf{6}$). One molecular precursor, $[\text{Os}(\text{bpy})_2(\text{C}_2\text{P}_2)_2](\text{PF}_6)_2$ ($\mathbf{5}$), was also prepared and reported herein. Their electronic absorption, steady-state and time-resolved emission spectroscopy, and quantum yields are investigated and compared here. The photoluminescent

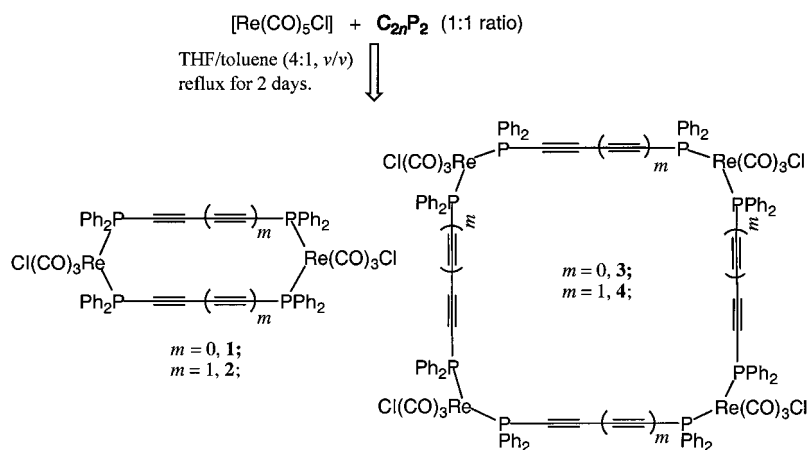
[a] Prof. Dr. B. Hong, D. Xu, K. T. Khin, Dr. W. E. van der Veer, Dr. J. W. Ziller
Department of Chemistry, University of California
Irvine, CA 92697-2025 (USA)
Fax: (+1) 949-824-3168
E-mail: bhong@uci.edu



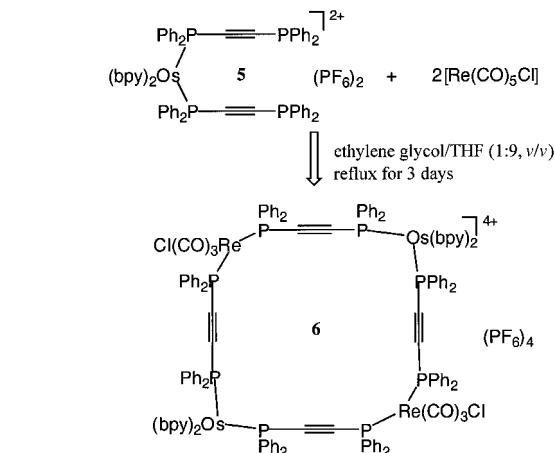
quantum yields (QY) of complexes **5** and **6** with Os^{II} centers are found to be much higher than those of the well-known complexes $[\text{M}(\text{bpy})_3](\text{PF}_6)_2$ ($M = \text{Ru}^{\text{II}}$ or Os^{II}). In addition, a guest-inclusion study using mixed-metal receptor **6** has been performed using different guests with increasing molecular sizes: anisole, 1,4-dimethoxybenzene, and 1,3,5-trimethoxybenzene. The size dependence of the host-guest binding constant (K_b) for these guest molecules will be addressed and compared with other macrocyclic receptors containing different metal centers.

Results and Discussion

Synthesis and purification: Homometallic **1–4** compounds were made by reactions between the suitable spacer C_{2n}P_2 ($n = 1, 2$) and $[\text{Re}(\text{CO})_5\text{Cl}]$ (1:1 ratio) in a refluxing THF/toluene solvent mixture (4:1 v/v, Scheme 1). The final products contain both dimeric and tetrameric metalloporphyrins. The dimers **1** and **2** were separated from the tetramers **3** and **4** using silica gel chromatography with different ratios of CH_2Cl_2 /hexanes mixtures as eluants. Since the dimers and tetramers with Re^{I} centers are neutral molecules and they also have relatively low solubility in common organic solvents, up to three cycles of column chromatography were needed, and this resulted in relatively low separation yields (10–20% after separation). The monometallic precursor **5** was prepared from $[\text{Os}(\text{bpy})_2(\text{CO})_3]$ using an excess amount of C_2P_2 . Since C_2P_2 is a ditopic ligand and capable of further binding to the second metal center, the yield of the desired monometallic product **5** was 30% after the chromatographic separation. From the reaction between **5** and $[\text{Re}(\text{CO})_5\text{Cl}]$ (1:1 ratio, Scheme 2) the



heterometallic macrocyclic complex **6** was synthesized. Repeated attempts have been made to prepare the monometallic precursor $[\{\text{Os}(\text{bpy})_2(\text{C}_4\text{P}_2)\}_2](\text{PF}_6)_2$ in a similar way with a longer spacer. However, a bimetallic product with two terminal Os^{II} centers was found to be the favored product, which has a ^{31}P NMR singlet at approximately $\delta = 30$. In addition, the ^{31}P NMR study reveals that these complexes with ditopic phosphanes are stable in air, and no oxidized species are observed.



Scheme 2. Synthesis of heterometallic complex **6**.

Characterization: X-ray quality crystals of the dimeric complex **1** were obtained by slow evaporation of THF at low temperature (4°C), and the crystal structure is shown in Figure 1a. Crystallographic data and data collection parameters are provided in Table 1. Selected bond lengths and bond angles are given in Table 2. The molecule is located about an inversion center, with two THF molecules present per dimeric formula unit. The molecule is slightly distorted, with $\text{P1}-\text{Re1}-\text{P2}$ as $90.15(2)^\circ$, $\text{C25}-\text{P1}-\text{Re1}$ as $115.04(9)^\circ$, and $\text{C26}-\text{P2}-\text{Re1}$ as $113.95(9)^\circ$. The angles of $\text{C25}'-\text{C26}-\text{P2}$ and $\text{C26}'-\text{C25}-\text{P1}$ are not linear but slightly bent with similar angles of $175.7(2)^\circ$ and $175.6(2)^\circ$, respectively. A 10-member ring is formed with two Re^{I} centers and two central C_2P_2 spacers. The distance between Re1 and Re2 is 7.466 \AA , and the average distance of $\text{P} \cdots \text{P}$ (e.g. P1 to P2) is 3.494 \AA . In addition, these molecules are found to align very well on top of each other (Figure 1b), and the solvent THF molecules locate between stacks of dimeric molecules. As a comparison, similar structural features have also been observed for $[\{\text{Pt}(\text{dppm})(\text{C}_2\text{P}_2)\}_2](\text{OTf})_4$,^[4b] with the observed $\text{Pt} \cdots \text{Pt}$ and $\text{P} \cdots \text{P}$ distances of 7.2 and 3.5 \AA , respectively.

A molecular modeling study was also performed to estimate the cavity dimension. All model structures were minimized using the Spartan builder, and the

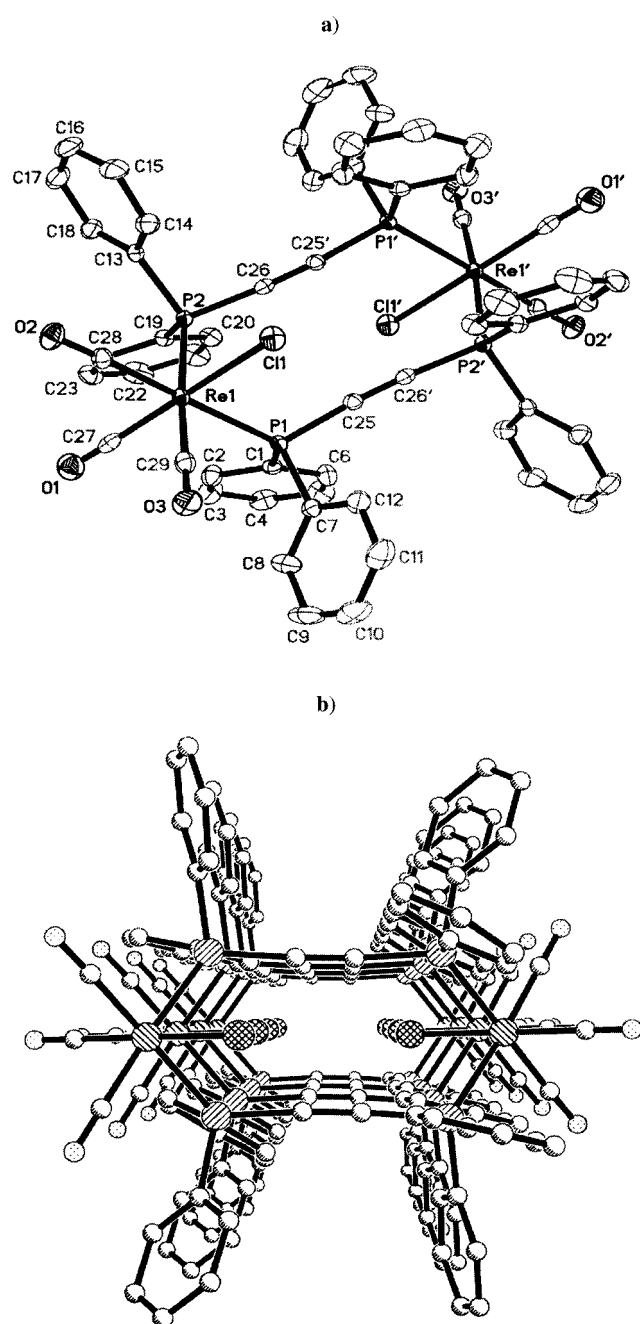


Figure 1. a) ORTEP of **1**; b) Stacking of molecules of **1** in one dimension.

representative stick-and-ball diagrams of metallocyclic complexes **3**, **4**, and **6** are shown in Figure 2. Interestingly, the homometallic tetramers **3** and **4** adopt “square-like” structures with the average Re...Re edge distance of 7.4 and 9.3 Å, and the average diagonal Re...Re distances of 9.3 and 9.9 Å, respectively. But the heterometallic **6** has an elongated “rhombic-shaped” structure with a longer Os...Os distance of 13.8 Å and a compressed Re...Re diagonal distance of 7.7 Å. Presumably the structural difference in **6** is caused by the presence of bulkier bpy ligands on Os^{II} centers. Another notable feature is that all Cl ligands are located “inside” toward the cavity in the structures or models obtained from the molecular modeling study and the aforementioned crystal

Table 1. Crystallographic data and data collection parameters for **1**.

formula	C ₆₆ H ₅₆ Cl ₂ O ₈ P ₄ Re ₂ (1 +2THF)
<i>M_r</i>	1544.29
<i>T</i>	158 K
<i>λ</i>	0.71073 Å
crystal system, space group	monoclinic, <i>P2₁/n</i>
unit cell dimensions	<i>a</i> = 12.8700(7) Å <i>α</i> = 90° <i>b</i> = 10.2006(5) Å <i>β</i> = 99.0640(10)° <i>c</i> = 23.2767(12) Å <i>γ</i> = 90°
crystal size	0.30 × 0.10 × 0.07 mm
volume, <i>Z</i>	3017.6(3) Å ³ , 2
density (calculated)	1.700 mg m ⁻³
absorption coefficient	4.258 mm ⁻¹
<i>F</i> (000)	1520
goodness-of-fit on <i>F</i> ²	1.036 ^[a]
final <i>R</i> indices [<i>I</i> > 2σ(<i>I</i>)]	<i>R</i> 1 = 0.0226, <i>wR</i> 2 = 0.0472 ^[a]
largest diff. peak and hole	0.968 and -0.603 e Å ⁻³

[a] *R*1 = Σ||*F_o*| - |*F_c*|| / Σ|*F_o*|; *wR*2 = [Σ*w*|*F_o*| - |*F_c*|]² / Σ*w*|*F_o*|²]^{1/2}, *w* = 1/*σ*²(*F_o*); goodness-of-fit = [Σ*w*|*F_o*|² - |*F_c*|²]² / (n - *p*)^{1/2}, where *n* is the number of reflections and *p* is the total number of parameters refined.

Table 2. Selected bond lengths [Å] and angles [°] for **1**.

Re1–C28	1.959(3)	P1–C1	1.823(3)
Re1–C29	1.964(3)	P1–C7	1.828(3)
Re1–C27	1.984(3)	P2–C26	1.767(3)
Re1–P2	2.4593(7)	P2–C19	1.818(3)
Re1–P1	2.4761(7)	P2–C13	1.834(3)
Re1–Cl1	2.4762(7)	C25–C26	1.196(4)
P1–C25	1.769(3)		
C28–Re1–C29	89.71(11)	C28–Re1–P1	177.34(8)
C28–Re1–C27	86.71(11)	C29–Re1–P1	88.66(8)
C29–Re1–C27	89.00(11)	C27–Re1–P1	95.37(8)
C28–Re1–P2	91.33(8)	P2–Re1–P1	90.15(2)
C29–Re1–P2	175.72(8)	C28–Re1–Cl1	91.87(8)
C27–Re1–P2	95.20(8)	C29–Re1–Cl1	89.04(8)
P2–Re1–Cl1	86.77(2)	C29–Re1–Cl1	89.04(8)
P1–Re1–Cl1	86.00(2)	C27–Re1–Cl1	177.59(8)
C26–P2–Re1	113.95(9)	C25–P1–Re1	115.04(9)
C25'–C26–P2	175.7(2)	C26'–C25–P1	175.6(2)

structure determination. Possible isomers may exist, where Cl ligands may point “inside” and/or “outside”, especially in complexes with two or four Re^I centers, however, this is not observed in the crystal structure of **1** and the molecular modeling study. This may partially be due to the fact that the Re–Cl unit is shorter or smaller than the Re–CO unit, and a less crowded structure may be obtained when the Cl ligands locate “inside”. However, we are not completely certain about what isomers we have for all our new complexes without crystallographic data, and we also cannot exclude the possibility that other isomers may indeed form but are lost during the chromatographic separation or crystallization procedures.

A ³¹P{¹H} NMR study gave one peak for each Re^I-based homometallic compound: δ = -9.0 for **1**, -12.9 for **2**, -14.5 for **3**, and -15.6 for **4**. These results suggest that all P atoms in each complex are in the identical environment. The precursor **5** has two peaks: δ = -9.8 for the Os^{II}-PPh₂ unit and -30.9 for the free -PPh₂ unit. Complex **6** was also found to

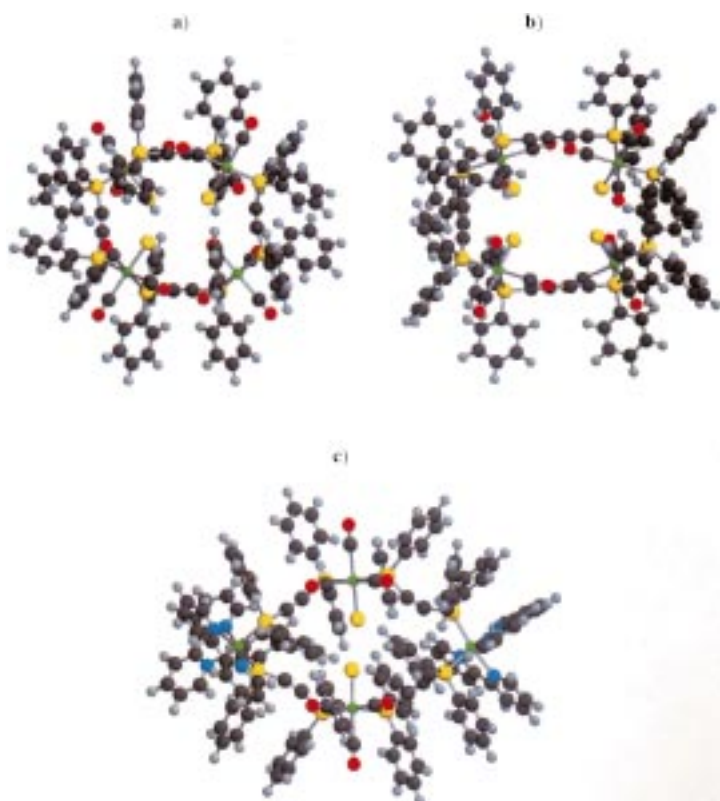


Figure 2. Molecular modeling study of complexes: a) **3**; b) **4**; c) **6**.

have two ^{31}P NMR signals: $\delta = -8.3$ for two Re^{I} -binding PPh_2 and $\delta = -9.1$ for two Os^{II} -binding PPh_2 . In addition, satisfactory elemental analysis data were obtained for all complexes. Specifically, the presence of water molecules was observed in the two complexes with Os^{II} centers, **5** and **6**, since they were initially precipitated out of the aqueous KPF_6 solution.

Both FAB/MS and ESI/MS methods prove to be successful in the identification of all new metallocyclic complexes. Several representative features arise when we compare the data.

- 1) All fragments observed in the FAB/MS analysis have a +1 charge, while fragments with multiple charges are observed in the ESI/MS analysis, especially for complex **6** with the presence of Os^{II} centers. As a comparison, FAB/MS provided two high molecular weight fragments for **6**: m/z : 3354 $[\text{6} - 3\text{PF}_6 + \text{O}]^+$ and 2479 $[\text{6} - \text{Re}(\text{CO})_3\text{Cl}(\text{C}_2\text{P}_2)_2 - 2\text{CO} - \text{PF}_6]^+$. However, ESI/MS analysis gave very strong multiple charged peaks: $[\text{6} - 3\text{PF}_6 - \text{Cl}]^{2+}$ at m/z : 1650.5 and $[\text{6} - 4\text{PF}_6 - \text{Cl}]^{3+}$ at 1051.7 (Figure 3). The inset of Figure 3 displays a close match between the simulated and observed isotope patterns for the fragment $[\text{6} - 4\text{PF}_6 - \text{Cl}]^{3+}$, where the isotope peaks are separated by 0.3–0.4 m/z units.
- 2) Although the fragments observed in the FAB and ESI analyses of each complex are different, the loss of CO, Cl, Ph, as well as the counteranion PF_6^- in $\text{Re}^{\text{I}}/\text{Os}^{\text{II}}$ species is common, in addition to the observation of molecular ions. For example, complexes **1** and **2** gave the molecular ion peaks $[\text{M}]^+$ at m/z : 1401 and 1449, respectively, and the subsequent fragments at m/z : 1365 $[\text{1} - \text{Cl}]^+$, 1337 $[\text{1} - \text{Cl} - \text{CO}]^+$, or 1421 $[\text{2} - \text{CO}]^+$ and

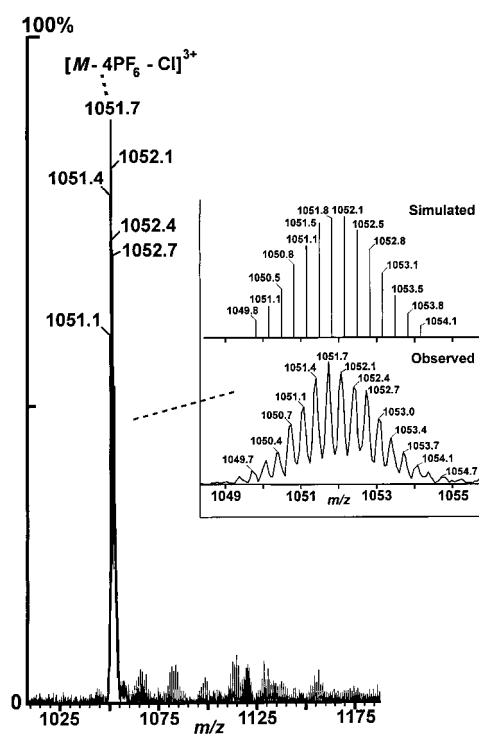


Figure 3. ESI mass spectrum for **6**: Inset is the comparison of the simulated and observed isotope pattern for the fragment $[\text{6} - 4\text{PF}_6 - \text{Cl}]^{3+}$.

1385 $[\text{2} - \text{CO} - \text{Cl}]^+$. The corresponding FAB/MS analysis of **3** and **4** gave the highest molecular fragment as $[\text{M} - \text{Cl}]^+$ and the subsequent loss of Ph and/or CO groups.

- 3) The addition of O and Na units was also observed. Previously in the mass spectral study of the molecular systems with polyphosphane spacers or ligands, the addition of extra O and Na also occurred.^[9, 10] These peaks are attributed to the strong complexing properties of the fragments with alkali metal cations and oxygen.

IR spectroscopy has been used to analyze the complexes with $[\text{Re}(\text{CO})_3\text{Cl}]$ moieties. Complexes **1–4** and **6** display the same three peaks pattern within the CO stretching region $1904\text{--}2038\text{ cm}^{-1}$: 2034, 1961, 1906 cm^{-1} for **1**; 2035, 1959, 1905 cm^{-1} for **2**; 2032, 1958, 1904 cm^{-1} for **3**; 2038, 1959, 1907 cm^{-1} for **4**; 2037, 1965, 1918 cm^{-1} for **6**. Previously, monomeric complexes of the type *fac*- $[\{\text{Re}(\text{CO})_3\text{Cl}(\text{phosphane})_2\}]$ were also reported to have similar three peaks patterns.^[11a] In the aforementioned X-ray crystal structure of the dimeric complex **1**, it was observed that each Re^{I} center independently possessed C_s symmetry with the three carbonyl ligands in a facial arrangement, one carbonyl *trans* to the chlorine atom, and the other two *trans* to the two phosphanes (Figure 1). Three IR-active ν_{CO} modes ($2A' + A''$) are expected for the Re^{I} centers that contain the local C_s symmetry.^[11b, c] Here, the highest energy peaks between $2032\text{--}2038\text{ cm}^{-1}$ represent the stretching of CO *trans* to the chlorine atom; the two lower energy peaks between $1904\text{--}1965\text{ cm}^{-1}$ are from the other two CO groups *trans* to PPh_2 units. Since the phosphanes are more electron-donating than Cl^- , stronger π -backbonding from the Re^{I} center to the CO *trans* to PPh_2 results in a lower bond order within the CO units that causes

ν_{CO} to shift to lower energies.^[11d, e] Hence, the IR study, in addition to the X-ray structure determination, confirms the facial arrangement of the three CO ligands on each Re^I center.

Electronic absorption: Metallo-cyclic complexes **1–4** exhibit two strong absorption peaks at 311–317 nm ($\epsilon = 8340$ – $19820 \text{ cm}^{-1} \text{ M}^{-1}$) and 340–346 nm ($\epsilon = 3070$ – $8310 \text{ cm}^{-1} \text{ M}^{-1}$, Table 3). Specifically, **1** and **3** have similar absorption spectra,

Table 3. Photophysical data for **1–4** in CH_2Cl_2 and **5–6** in CH_3CN .

	$\lambda_{\text{abs}} (\epsilon) \text{ nm} [\text{cm}^{-1} \text{ M}^{-1}]$	$\lambda_{\text{em}} [\text{nm}]$	$\tau [\text{ns}, \pm 5\%]$	$\Phi \times 10^4 [\pm 10\%]$	$k_r^{[e]} [\text{s}^{-1}]$	$k_{\text{nr}}^{[f]} [\text{s}^{-1}]$
1	311 (8340) 340 (3070)	525 ^[a]	3.4 ^[b]	3.8 ^[c]	1.1×10^6	2.9×10^8
2	317 (9005) 345 (4265)	510 ^[a]	6.8 ^[b]	4.5 ^[c]	6.6×10^5	1.5×10^8
3	311 (18670) 341 (8280)	525 ^[a]	3.8 ^[b]	6.8 ^[c]	1.8×10^6	2.6×10^8
4	317 (19820) 346 (8310)	505 ^[a]	3.0 ^[b]	8.4 ^[c]	2.8×10^6	3.3×10^8
5	289 (34820) 424 (7480) 470 (2850) 565 (1550)	605 ^[d]	675 ^[d]	2500 ^[d]	3.8×10^5	1.1×10^6
6	291 (72020) 420 (14095) 470 (5220) 560 (2800)	600 ^[d]	650 (Os ^{II}) ^[d]	1700 ^[d]	2.7×10^5	1.3×10^6

[a] The same emission maximum was obtained when $\lambda_{\text{ex}} = 350, 400$ – 488 nm . [b] $\lambda_{\text{ex}} = 488 \text{ nm}$, obtained on a SLM-Aminco 48000 MHF Fourier Transform Spectrofluorometer. [c] $\lambda_{\text{ex}} = 400 \text{ nm}$, referenced to a dilute quinine sulfate water solution with H_2SO_4 (0.2 M) ($\Phi = 0.55$ at 293 K).^[21] [d] $\lambda_{\text{ex}} = 470 \text{ nm}$, referenced to $[\text{Ru}(\text{bpy})_3](\text{PF}_6)_2$ ($\Phi = 0.062$ in CH_3CN at 293 K).^[8a] [e] Radiative decay rate $k_r = \Phi/\tau$.^[8d] [f] Nonradiative decay rate $k_{\text{nr}} = 1/\tau - k_r$.^[8d]

as well as **2** and **4**, and the tetramers have extinction coefficients that are approximately twice that of the dimers with the same spacers. Previously, $[\text{ReCl}(\text{CO})_5]$,^[12a] $[\text{ReCl}(\text{CO})_4(\text{PPh}_3)]$,^[12b, c] and $[\text{ReCl}(\text{CO})_3(\text{PPh}_3)_2]$ ^[11a] were reported to have two absorption peaks within 290–370 nm: one is ligand-centered absorption (LC) and the other is ligand-field absorption (LF). Such assignment in the literature was made based on the fact that these monometallic complexes did not have low-lying π -antibonding orbitals to participate in the MLCT (Metal-to-Ligand Charge Transfer) transition, and their low extinction coefficients ($< 20 \text{ M}^{-1} \text{ cm}^{-1}$) were consistent with a spin forbidden d–d transition. In our current system with C_{2n}P_2 spacers, the first stronger peak at 311–317 nm is assigned to the LC state. However, the second band (340–346 nm) is ascribed to the ¹MLCT transition (Re^I to C_2P_2 or C_4P_2 charge transfer) instead of a LF transition. This assignment of the lower energy absorption band is based on the fact that this band has relatively high extinction coefficients of 3070 – $8310 \text{ M}^{-1} \text{ cm}^{-1}$ which contradicts the assignment of a forbidden d–d transition in this system. The parent complex, $[\text{Re}(\text{CO})_5\text{Cl}]$, was also known to be luminescent from a d–d state.^[12a] However, upon replacement of two CO ligands with polypyridines (e.g. bipyridine or *o*-phenanthroline), the lowest excited state was reported as a metal-to-ligand charge transfer state.^[11a, 12a, 13] The polyphos-

phane/poly-yne spacers used in this study, similar to polypyridyl ligands, most likely possess low-lying rings and poly-yne π -antibonding orbitals that are capable of participation in charge-transfer interactions. Hence, a MLCT state is assigned as the emitting excited state based on the literature study and the observed extinction coefficients. Similarly a Re^I → phosphane charge-transfer band was also observed in our recent study on one-dimensional systems with polyphosphane/cumulene spacers.^[13c]

Monomeric precursor **5** and **6** have three absorption peaks between 400–800 nm: the ones at 420–424 nm ($\epsilon = 7480$ – $14095 \text{ M}^{-1} \text{ cm}^{-1}$) and 470 nm ($\epsilon = 2850$ – $5220 \text{ M}^{-1} \text{ cm}^{-1}$) are assigned to the bands of Re^I and Os^{II} ¹MLCT absorption. The third one at 560–565 nm ($\epsilon = 1550$ – $2800 \text{ M}^{-1} \text{ cm}^{-1}$) was assigned to the ³MLCT absorption. In addition, one higher energy band at 289–291 nm is also observed, which can be ascribed to the mixture of LC bands from both Re^I and Os^{II} centers. Overall the peak positions in the absorption spectra of **3**, **4**, and **6** are very similar to those of **1**, **2**, and **5**, respectively, but with approximately doubled extinction coefficients, which are indicative of a chromophore summation effect.^[10a, 14]

Molecular photophysics: A steady-state luminescence study at room temperature resulted in emission at $\lambda_{\text{em}} = 525, 510, 525,$ and 505 nm for **1**, **2**, **3**, and **4**, respectively, upon excitation at 450 nm (Table 3). At excitation wavelengths 350 and 400–488 nm, the same emission peak was observed. The parent complex $[\text{Re}(\text{CO})_5\text{Cl}]$ was reported to have emission from a d–d state at a maximum of 19900 cm^{-1} (502 nm).^[12] The emission bands for $[\text{Re}(\text{CO})_4\text{Cl}(\text{P})]$ and $[\text{Re}(\text{CO})_3\text{Cl}(\text{P})_2]$ complexes (P = phosphanes, e.g. PPh_2Me) were also assigned to the ligand-field d–d transition.^[11a, 12] However, since the lowest excited state in **1–4** is assigned to the MLCT band as discussed previously, the nature of the observed emission here is therefore attributed to the Re^I → C_{2n}P_2 ($n = 1, 2$) charge-transfer band.

The lifetimes, quantum yields, radiative and nonradiative rate constants (k_r and k_{nr} , respectively) are measured or calculated as in Table 3. While short lifetimes of 3.4–6.8 ns were observed for the Re^I-based excited states, much longer lifetimes of 650–675 ns were found for the Os^{II} metal-to-ligand charge-transfer band (triplet in nature). Interestingly, both the lifetime and quantum yield of the Os^{II} centers in the heterometallic tetramer **6** are smaller than those of the monomeric precursor **5**. No steady-state and time-resolved emission from the Re^I-based excited state in **6** can be detected using our current setups with a measurable range of lifetime as

short as 200 ps. From the lifetime and quantum yield of each complex, the radiative and nonradiative decay constants can be calculated using $k_r = \Phi/\tau$ and $k_{nr} = 1/\tau - k_r$.^[8d, f] Notably the Re^I excited-state decay is dominated by the nonradiative decay with k_{nr} of $1.5 - 3.3 \times 10^8 \text{ s}^{-1}$, while much lower k_{nr} values of $1.1 - 1.3 \times 10^6 \text{ s}^{-1}$ were observed for the Os^{II} excited state.

Previously the monomeric Os^{II} complexes with phosphanes, such as PPh₂Me and dpmm (dpmm = Ph₂PCH₂PPh₂), have been studied to probe the relationship of k_{nr} versus emission energy.^[8c, f] As compared in Table 4, a systematic trend exists

Table 4. Comparison of photophysical data of Os^{II} species with phosphanes.

Complexes ^[a]	E_{em} [cm ⁻¹]	τ [ns]	Φ	k_{nr} [s ⁻¹]
[Os(bpy) ₃ (PF ₆) ₂] ^[8c-e, 8f]	13 423	60	0.00461.7 × 10 ⁷	
[Os(bpy) ₂ (PPh ₂ Me) ₂](PF ₆) ₂ ^[8f]	15 106	260	0.026	3.7 × 10 ⁶
[Os(bpy) ₂ (dpmm)](PF ₆) ₂ ^[8c, d]	15 528	304	0.056	3.1 × 10 ⁶
[Os(bpy) ₂ (dppe)](PF ₆) ₂ ^[8f]	15 625	462	0.055	2.0 × 10 ⁶
[Os(bpy) ₂ (dppb)](PF ₆) ₂ ^[8d, 15b]	15 723	344	0.049	2.8 × 10 ⁶
[Os(bpy) ₂ (dppene)](PF ₆) ₂ ^[8c, d]	15 873	500	0.070	1.9 × 10 ⁶
[Os(bpy) ₂ (C ₂ P ₂) ₂](PF ₆) ₂ (5)	16 529	675	0.25	1.1 × 10 ⁶
[{Re(CO) ₃ Cl] ₂ [Os(bpy) ₂] ₂ (C ₂ P ₂) ₄](PF ₆) ₄ (6)	16 667	650	0.17	1.3 × 10 ⁶

[a] bpy = 2,2'-bipyridine, dpmm = Ph₂PCH₂PPh₂, dppe = Ph₂PCH₂CH₂PPh₂, dppb = 1,2-(PPh₂)₂C₆H₄, dppene = *cis*-Ph₂PCH=CHPPh₂, C₂P₂ = Ph₂PC≡CPh₂.

in which the quantum yield and lifetime of the Os^{II} excited state increase significantly as the ³MLCT emission energy increases in a series of Os^{II} species with auxiliary bpy ligands and various phosphanes. To the best of our knowledge, compound **6** represents the first type of luminescent Os^{II} heterometalocyclic complex with extraordinarily strong photoluminescence. Specifically, remarkable quantum yields as high as 0.25 (ca. four times of QY of [Ru(bpy)₃(PF₆)₂]^[8a] and 54 times of [Os(bpy)₃(PF₆)₂]^[8c, d, f] and 0.17 (2.7 times of [Ru(bpy)₃(PF₆)₂] and 37 times of [Os(bpy)₃(PF₆)₂]) were observed for **5** and **6**, respectively. These QY values are also much higher than the other Os^{II} species with phosphanes as listed in Table 4. It appears that the role of ligands in determining the excited-state lifetimes and quantum yields is in its electronic effect on the metal, and the replacement of one of the bpy groups by various phosphanes with π -accepting ability significantly affects the excited-state property.^[8c] Based on the observed data in this study and in the literature, we may evaluate the π -acceptor ability in the following order:^[8, 15] bipyridine < [CH₃(CH₂)₃]₃P < [*p*-CH₃C₆H₄]₃P ≈ CH₃Ph₂P < PPh₂CH₂PPh₂ (dpmm) < PPh₂CH₂CH₂PPh₂ (dppe) < 1,2-(PPh₂)₂-C₆H₄ (dppb) < *cis*-Ph₂PCH=CHPPh₂ (dppene) < Ph₂P-C≡C-PPh₂ (C₂P₂). As the π -acceptor ability of phosphanes increases, the energy gap between the ground and excited state increases, and this results in blue-shifted emission energy. As a consequence, the coupling between these two states decreases, and a lower nonradiative decay constant, k_{nr} , is observed (Table 4).

Previously the “energy-gap law” predicted that nonradiative decay rate constants for a series of related excited states based on the same chromophores are predominately determined by vibrational overlap between the ground and excited

states.^[8f] Specifically, using the expression derived by Englman and Jortner^[16] and at the low temperature, weak vibrational coupling limit ($S = 1$), the value of k_{nr} can be expressed approximately as Equation (1).^[16]

$$k_{nr} = \left(\frac{2\pi V^2}{\hbar} \right) \left(\frac{1}{2\pi\hbar\omega_M\Delta E} \right)^{1/2} \exp(-S) \exp\left(\frac{-\gamma\Delta E}{\hbar\omega_M} \right) \quad (1)$$

In this equation ΔE is the internal energy gap between the upper and lower states, ω_M is the frequency of the deactivation mode or modes, V is the electron-tunneling matrix element, and the terms γ and S are defined in Equations (2) and (3).^[8f] When the deactivating mode or modes remain common and if variations in V and S are relatively small, as is the case for the [Os(bpy)₂(L)₂]²⁺ type of complexes,^[8f, 18] then Equation (1) can be written as Equation (4), on the assumption that $\Delta E \approx E_{em}$ and Δ_j is the dimensionless fractional replacement between the equilibrium nuclear configuration of the ground and excited state for the complex's j th normal mode.^[8f, 17]

$$\gamma \approx \ln \left(\frac{2\pi\Delta E}{\hbar\omega_j\Delta_j^2} \right) - 1 \quad (2)$$

$$S = 1/2 \sum_j \Delta_j^2 \quad (3)$$

$$\ln k_{nr} = (\ln\beta - S) - \left(\frac{\gamma E_{em}}{\hbar\omega_M} \right) \quad (4)$$

If all the assumptions above are valid a linear relationship should exist between $\ln k_{nr}$ and E_{em} . Indeed from the plot of $\ln k_{nr}$ versus E_{em} (Figure 4) a linear fit is obtained, which is

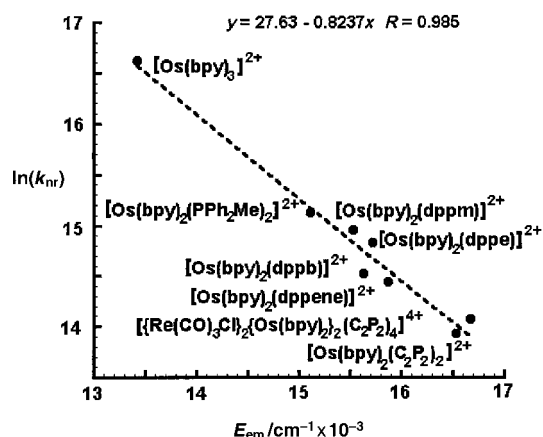


Figure 4. Plot of E_{em} versus $\ln(k_{nr})$, where E_{em} is the emission energy, and k_{nr} is the nonradiative decay rate constant.

indicative of good agreement between the theory and experiments. From this linear fit a slope of $(-0.82 \pm 0.04) \times 10^3 \text{ cm}^{-1}$ and an intercept of (27.6 ± 0.3) are obtained for the series of Os^{II} complexes with phosphanes, including complexes **5** and **6** from this study. These values are consistent with those previously found for polypyridyl Ru^{II} and Os^{II} complexes, in which the change of E_{em} was caused by replacing the nonchromophoric ligands.^[8c, d, f] Therefore we may conclude that: a) The fact that the data of both complexes **5** and **6** fit in with the other [Os(bpy)₂(P)₂] or [Os(bpy)₂(PP)] (P = monophosphanes, PP = biphosphanes) types of complex suggests that the emitting excited states of these complexes share a

common deactivation mode or modes, b) A clear trend exists in Table 4 that as k_{nr} decreases both the lifetime and quantum yield increase. The aforementioned discussion has stated that the replacement of one bpy ligand by various phosphanes with different π -accepting ability increases the energy gap between the excited and ground state which results in a decrease in k_{nr} values. Although the same phosphane C_2P_2 is employed in both **5** and **6**, the attachment of $[Re(CO)_3Cl]$ units at the opposite termini may cause changes in the electronic effect and π -acceptor property of the phosphane. Hence, the difference in the emission maxima and quantum yields between **5** and **6** may be ascribed to the changes in the structures and, as a consequence, changes in the π -acceptor ability of phosphanes and nonradiative decay constant of the emitting excited state.

Energy transfer: When we compare the emission maxima of complexes **5** and **6**, observed at 605 and 600 nm, both originated from the Os^{II} 3MLCT excited state. In addition, excitation at wavelengths of 350 and 400–550 nm results in the same emission peak. The absence of emission from the $[Re(CO)_3Cl(P)_2]$ type of chromophore in heterometallic **6** suggests possible energy transfer from the Re^I unit to the Os^{II} center. When we compared the absorption and emission spectra of complex **6**, substantial overlap was observed as in Figure 5. In addition, the emission of Re^I chromophores (ca. 505–525 nm) used in this series of complexes also has

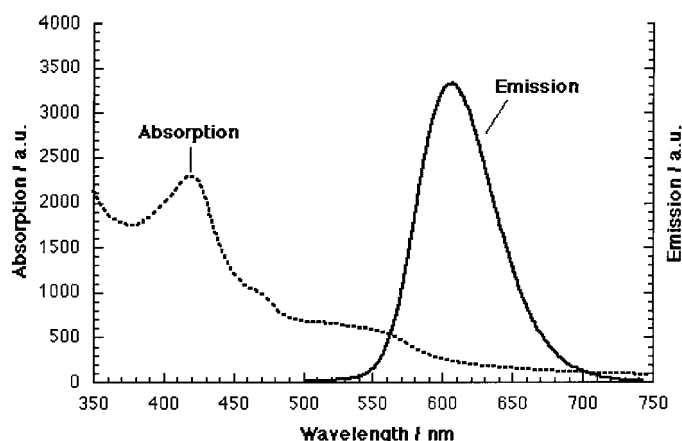


Figure 5. Overlap of the absorption and emission spectra of **6**.

substantial overlap with the absorption of the Os^{II} chromophore in the visible range (ca. 420–565 nm). Furthermore, following the conventional assumptions,^[19] the driving force for the energy transfer, ΔG^\ominus , can be estimated using the spectroscopic energies of the donor and acceptor emission, $\Delta G^\ominus = \lambda_{em}(donor) - \lambda_{em}(acceptor)$. The ΔG^\ominus value thus calculated is -2520 cm^{-1} or -0.31 eV , which is indicative of a thermodynamically favored energy-transfer process. Since the lifetime of the Re^I donor was not detected using our current setups with a measurable lifetime as low as 200 ps, we may estimate the energy-transfer rate constant as $>4.7 \times 10^9\text{ s}^{-1}$ using Equation (5).^[19, 20]

$$k_{en} = 1/\tau - 1/\tau_m \quad (5)$$

Here τ is the quenched lifetime of the Re^I energy donor in **6** ($<200\text{ ps}$), and τ_m is the lifetime of model complex **3** (3.8 ns). All the evidence and calculations suggest an efficient energy transfer from the Re^I -based donor to the Os^{II} -based acceptor.

Host–guest chemistry: As shown in the aforementioned X-ray structure determination and molecular modeling study, the metallocyclic species have cavity sizes that are different if metal corner units and spacers are changed. However, the Re^I -based complexes have relatively low emission efficiency, and the change in emission intensity, upon addition of a guest molecule, was not significant. Hence, only the host–guest study using heterometallic species **6** is reported here, using anisole, 1,4-dimethoxybenzene, and 1,3,5-trimethoxybenzene as the guest molecules. Experimentally when the guest was added quantitatively to the host solution (total volume change is $<5\%$), the decrease of emission intensity at 600 nm was monitored and recorded (Figure 6).

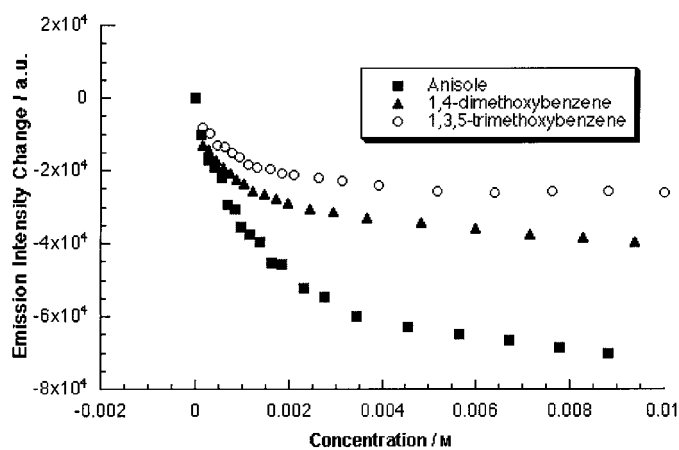


Figure 6. Emission intensity changes of **6** versus the concentrations of three guests: anisole, 1,4-dimethoxybenzene, and 1,3,5-trimethoxybenzene. Concentration of the host is $6.2 \times 10^{-5}\text{ M}$ in MeCN.

To obtain the host–guest binding constant, the change of emission intensity is fitted as a function of the guest concentration to Equation (6).^[1d]

$$I = I_0 + \Delta I * K_b * C / (1 + K_b * C) \quad (6)$$

Here I_0 and ΔI are the initial emission intensity of the host molecule and the extrapolated maximum intensity change, and C is the concentration of the guest. This binding constant expression is valid when the guest concentration is significantly higher than the concentration of the host, and the binding molecularity and stoichiometry are both 1:1.^[1d] The calculated values of K_b for anisole, 1,4-dimethoxybenzene, and 1,3,5-trimethoxybenzene are 775 M^{-1} , 1580 M^{-1} , and 1680 M^{-1} , respectively. A direct relationship between the guest molecular size and the host–guest binding constant is observed here, and K_b increases as the guest size increases. Furthermore, when compared with the host–guest binding constants in the previous guest-inclusion study using the molecules anisole and 1,4-dimethoxybenzene as guests and different host molecules such as macrocyclic dimer $[[Pt-$

(dppm)₂(C₂P₂)₂(OTf)₄,^[4b] dimer $[\{\text{Ru}(\text{tpy})\text{Cl}\}_2(\text{C}_4\text{P}_2)_2](\text{PF}_6)_2$,^[4a] and trimer $[\{\text{Ru}(\text{tpy})\text{Cl}\}_3(\text{C}_4\text{P}_2)_3](\text{PF}_6)_3$,^[4a] (Table 5, C₄P₂ = Ph₂P–C≡C–C≡C–PPh₂, C₂P₂ = Ph₂P–C≡C–PPh₂), the binding constant K_b was found to be susceptible to a change of cavity dimensions. Interestingly, for the macrocyclic dimer and trimer with [Ru(tpy)(P)₂Cl] units, the host emission intensity (I) increased upon addition of guest anisole or 1,4-dimethoxybenzene.^[4a] However, for metalocycles with Re^I/Os^{II} or Pt^{II} centers, the opposite changes were observed that the I value decreased as guest concentration increased. Furthermore, a comparison of the K_b values for an anisole guest in Table 5 reveals the trend of an initial increase and then a decrease in K_b as the cavity size is increased. Despite the structural and charge differences in these complexes, the largest K_b value (2370 M⁻¹) suggests a best match between the host cavity of $[\{\text{Ru}(\text{tpy})\text{Cl}\}_3(\text{C}_4\text{P}_2)_3](\text{PF}_6)_3$ with an anisole molecule. For the larger 1,4-dimethoxybenzene, K_b increases as a function of cavity size, which is indicative of a better match of this molecule with the larger cavity in the heterometallic complex **6**. Such correlation between the cavity size, guest molecular size, and the host–guest binding constant (K_b) may suggest the inclusion of guest molecules within the host cavities.

Conclusion

We have found that rigid ditopic phosphanes with short polyyne chains are excellent spacers in the construction of photoactive metalocyclic supramolecules. Specifically, the strongly luminescent molecules with octahedral Re^I/Os^{II} centers can be prepared, with the lowest excited state assigned as the ¹MLCT for Re^I and ³MLCT for Os^{II}. All Re^I macrocycles **1–4** have two strong LC and MLCT absorption peaks, and complexes **5** and **6** with Os^{II} centers exhibit additional characteristic MLCT bands for Os^{II} centers. In addition, a chromophore summation effect is also observed in the extinction coefficients of the absorption bands in these new complexes; the effect is indicated by the amount of chromophores in the tetramer which is double that in the dimer. Emission maxima of **1–4** were found to be very blue-shifted when compared with those of **5** and **6**, and their shorter lifetimes and low quantum yields result from the singlet MLCT excited states with a high nonradiative decay constant of 1.5–3.3 × 10⁸ s⁻¹. In contrast, significantly high quantum yields of 0.25 and 0.17 were measured for **5** and **6**. In addition, energy transfer from Re^I to Os^{II} is also evidenced with an

estimated driving force ΔG^\ominus of approximately –0.31 eV and a rate constant of >4.7 × 10⁹ s⁻¹. A guest inclusion study using macrocyclic receptor **6** reveals a dependence of binding constant (K_b) on the size of guest molecules, with larger K_b values observed for larger guests when a series of molecules, anisole, 1,4-dimethoxybenzene, and 1,3,5-trimethoxybenzene, was used. When compared with other reported systems^[4] using the same rigid polyphosphane spacers such as Ph₂P–C≡C–PPh₂ or Ph₂P–C≡C–C≡C–PPh₂, we found that the cavity sizes can be tuned in the metalocyclic receptors with various metal centers such as Pd^{II}, Pt^{II}, Re^I, Ru^{II}, and/or Os^{II}. The binding constants for guest inclusion are also found to be sensitive to the cavity size. Such ability to modulate the cavity size by structural modification and consequently the tuning of binding constants and host–guest interaction is important for the design of this type of supramolecules for host–guest chemistry and selective molecular sensing.

Experimental Section

General methods: All experiments were performed under a nitrogen atmosphere using standard glove box and Schlenk techniques.

Materials: [Re(CO)₅Cl] (Strem), C₂P₂ (Strem), NH₄PF₆ (Acros), and KPF₆ (Acros) were purchased. C₄P₂^[4a] and [Os(bpy)₂(CO₃)]^[8b] were synthesized according to the literature methods. Tetrahydrofuran (THF) was distilled under nitrogen from solutions containing sodium benzophenone ketyl. Ethylene glycol and toluene were dried over 4 Å molecular sieves for at least 24 h and deoxygenated by degassing with dry N₂ for 20 min or longer prior to use. All spectrophotometric grade solvents and ACS grade solvents were purchased from Acros (Fisher) and used without further purification.

Physical measurements

NMR, EA, IR, and MS measurements: ³¹P{¹H} NMR spectra were obtained on an Omega 500 MHz spectrometer, referenced to a solution of H₃PO₄ (85 %) in D₂O. Combustion analysis data (C, H) of complexes **1–5** were collected from a Carlo Erba Instruments Fisons Elemental Analyzer. For complex **6**, the elemental analysis was done by Atlantic Microlab Inc. Infrared absorption spectra were recorded using a Nicolet Impact Model 410FT-IR with a DTGS (deuterated triglyme sulfate) detector. Fast atom bombardment mass spectral analysis (FAB/MS) data were obtained on a Micromass (Altrincham, UK) Autospec mass spectrometer at UCI Mass Spectral Facility. Cesium ions at 25 kV were the bombarding species, and the matrix was *meta*-nitro benzylalcohol (*m*-NBA). Electro-spray mass spectra (ESI/MS) were recorded on a Finnigan LCQ API mass spectrophotometer at Finnigan Corp. or on a Micromass LCTAPI-TOF mass spectrometer in UCI mass spectral facility.

Photophysical measurements: Absorption spectra were recorded on a Hewlett-Packard 8453 diode array spectrophotometer. Room temperature steady-state emission spectra were obtained on a Hitachi 4500 fluorescence spectrometer. Luminescence quantum yields (QY) of **1–4** were measured

Table 5. Binding constants using guest molecules anisole and 1,4-dimethoxybenzene.

Complex ^[a]	K_b , anisole [M ⁻¹] [± 5 %]	K_b , 1,4-dimethoxybenzene [M ⁻¹] [± 5 %]	Cavity dimension ^[b] [Å]
$[\{\text{Re}(\text{CO})_5\text{Cl}\}_2\{\text{Os}(\text{bpy})_2\}_2(\text{C}_2\text{P}_2)_4](\text{PF}_6)_4$ (6)	775	1580	13.8 (av. Os–Os) 7.7 (av. Re–Re) 8.1 (av. Os–Re)
$[\{\text{Ru}(\text{tpy})\text{Cl}\}_3(\text{C}_4\text{P}_2)_3](\text{PF}_6)_3$ ^[4a]	2370	1390	8.9 (av. Ru–Ru)
$[\{\text{Ru}(\text{tpy})\text{Cl}\}_2(\text{C}_4\text{P}_2)_2](\text{PF}_6)_2$ ^[4a]	220	250	7.2 (av. Ru–Ru) 5.0 (av. P–P)
$[\text{Pt}(\text{dppm})(\text{C}_2\text{P}_2)_2](\text{OTf})_4$ ^[4b]	310	60	7.2 (av. Pt–Pt) 3.5 (av. P–P)

[a] C₂P₂ = Ph₂P–C≡C–PPh₂, C₄P₂ = Ph₂P–C≡C–C≡C–PPh₂, dppm = Ph₂PCH₂PPh₂, tpy = 2,2',6',2''-terpyridine, and bpy = 2,2'-bipyridine. [b] Cavity dimension is determined using molecular modeling or crystal structure determination.

using dilute quinine sulfate water solution with H_2SO_4 (0.2 M) as reference ($\Phi = 0.55$ at 293 K^[21]), and OYs of **5** and **6** were standardized using $[\text{Ru}(\text{bpy})_3](\text{PF}_6)_2$ ($\Phi = 0.062$ in CH_3CN at 293 K^[81]).

The time-resolved emission spectroscopic studies were performed on a nanosecond laser flash photolysis unit equipped with a Continuum Surelite II-10 Q-switched Nd:YAG laser and a Surelite OPO (optical parametric oscillator) tunable visible source, a LeCroy 9350A Oscilloscope, and a Spex 270 MIT-2x-FIX high-performance scanning and imaging spectrometer. Only lifetimes longer than 6 ns were measured accurately with this setup. Lifetimes shorter than 6 ns were measured on a SLM-Aminco 48000 MHF Fourier Transform Spectrofluorometer. As a light source, the 488 nm line of a Coherent Innova 90 Argon ion laser was used. The laser beam was modulated with a comb function with an interval spacing of 5 MHz, with a maximum frequency of 250 MHz. The resulting beam was imaged on the sample; the resulting fluorescence was detected with a photomultiplier with a Schott filter (OG 515). The phase and intensity of each component of the comb function were determined; the required reference signal was obtained by the utilization of a small portion of the incident beam. The resulting signals were fitted with a single exponential, which obtained the best fit with respect to both the recorded phase and intensity information. For each sample a series of five measurements was obtained, each consisting of 1000 scans. The optical density (O.D.) used for the measurements was approximately 0.1–0.5.

Molecular modeling: Molecular modeling was performed on Silicon Graphics Indigo2 XZ workstations at UCI Molecular Modeling Facility, using Spartan V. 5.1.1-62 for IRIX developed by Wavefunction, Inc. All model structures were minimized using the Spartan builder. No solvent molecules or stacks of the metallocyclic molecules were used in the modeling study.

General preparation of dimeric (1, 2) and tetrameric (3, 4) Re^I complexes with C_2P_2 and C_4P_2 : A solution of 1:1 ratio of $[\text{Re}(\text{CO})_5\text{Cl}]$ and C_{2n}P_2 ($n = 1, 2$) in THF/toluene (125 mL, 4:1 v/v) was heated to reflux for two days. The light yellow mixture was cooled down to room temperature. The solvent was removed under reduced pressure using a cold finger, and the solid residue was re-dissolved in an minimum amount of THF and added dropwise to hexanes (100 mL) under vigorous stirring. The precipitate (white solids for complexes with C_2P_2 , and light yellow solids for the species with C_4P_2) was collected by filtration and dried in vacuo. Before separation by silica gel (70–230 mesh) chromatography using a CH_2Cl_2 /hexanes mixture as eluant (1:2 v/v for **1** and **2**, and 2:1 v/v for **3** and **4**), the total yield of the **1** and **3** mixture is 95 %, and the **2** and **4** mixture is 91 %. The yields of the individual compounds after column separation are recorded below. White needle crystals of **1** were obtained after slow evaporation of solvent THF at 4 °C. One of the crystals was used in the X-ray structure determination of **1**.

$[\{\text{Re}(\text{CO})_5\text{Cl}(\text{C}_2\text{P}_2)\}_2]$ (1**):** Yield: 20 %. $^{31}\text{P}\{^1\text{H}\}$ NMR (202 MHz, $\text{CH}_2\text{Cl}_2/\text{C}_6\text{D}_6$, 25 °C): $\delta = -9.0$ (s); FAB/MS: (m/z): 1401 $[\text{M}]^+$, 1365 $[\text{M} - \text{Cl}]^+$, 1337 $[\text{M} - \text{Cl} - \text{CO}]^+$; ESI/MS: (m/z): 1423 $[\text{M} + \text{Na}]^+$, 1365 $[\text{M} - \text{Cl}]^+$, 1337 $[\text{M} - \text{Cl} - \text{CO}]^+$; FT-IR: $\tilde{\nu}_{\text{CO}} = 2034, 1961, 1906\text{cm}^{-1}$; elemental analysis calcd (%) for $\text{C}_{58}\text{H}_{40}\text{O}_6\text{P}_4\text{Cl}_2\text{Re}_2$ (1400.13): C 49.76, H 2.88; found C 49.54, H 3.19.

$[\{\text{Re}(\text{CO})_5\text{Cl}(\text{C}_4\text{P}_2)\}_2]$ (2**):** Yield: 12 %. $^{31}\text{P}\{^1\text{H}\}$ NMR (202 MHz, $\text{CH}_2\text{Cl}_2/\text{C}_6\text{D}_6$, 25 °C): $\delta = -12.9$ (s); FAB/MS: (m/z): 1449 $[\text{M}]^+$, 1421 $[\text{M} - \text{CO}]^+$, 1385 $[\text{M} - \text{Cl} - \text{CO}]^+$; ESI/MS: (m/z): 1471 $[\text{M} + \text{Na}]^+$, 1412 $[\text{M} - \text{Cl}]^+$, 1231 $[\text{M} - \text{Cl} - \text{CO} - 2\text{Ph}]^+$; FT-IR: $\tilde{\nu}_{\text{CO}} = 2035, 1959, 1905\text{cm}^{-1}$; elemental analysis calcd (%) for $\text{C}_{62}\text{H}_{40}\text{O}_6\text{P}_4\text{Cl}_2\text{Re}_2$ (1448.18): C 51.42, H 2.78; found C 51.81, H 2.84.

$[\{\text{Re}(\text{CO})_5\text{Cl}(\text{C}_2\text{P}_2)\}_4]$ (3**):** Yield: 10 %. $^{31}\text{P}\{^1\text{H}\}$ NMR (202 MHz, $\text{CH}_2\text{Cl}_2/\text{C}_6\text{D}_6$, 25 °C): $\delta = -14.5$ (s); FAB/MS: (m/z): 2765 $[\text{M} - \text{Cl}]^+$, 2687 $[\text{M} - \text{Cl} - \text{Ph}]^+$, 2651 $[\text{M} - 2\text{Cl} - \text{Ph}]^+$; ESI/MS: (m/z): 2823 $[\text{M} + \text{Na}]^+$, 2550 $[\text{M} - 2\text{Cl} - \text{CO} - 2\text{Ph}]^+$; FT-IR: $\tilde{\nu}_{\text{CO}} = 2032, 1958, 1904\text{cm}^{-1}$; elemental analysis calcd (%) for $\text{C}_{116}\text{H}_{80}\text{O}_{12}\text{P}_8\text{Cl}_4\text{Re}_4$ (2800.27): C 49.76, H 2.88; found C 49.82, H 2.75.

$[\{\text{Re}(\text{CO})_5\text{Cl}(\text{C}_4\text{P}_2)\}_4]$ (4**):** Yield: 15 %. $^{31}\text{P}\{^1\text{H}\}$ NMR (202 MHz, $\text{CH}_2\text{Cl}_2/\text{C}_6\text{D}_6$, 25 °C): $\delta = -15.6$ (s); FAB/MS: (m/z): 2862 $[\text{M} - \text{Cl}]^+$, 2785 $[\text{M} - \text{Cl} - \text{Ph}]^+$, 2757 $[\text{M} - \text{Cl} - \text{Ph} - \text{CO}]^+$; ESI/MS: (m/z): 2920 $[\text{M} + \text{Na}]^+$, 2645 $[\text{M} - 2\text{Cl} - \text{CO} - 2\text{Ph}]^+$; FT-IR: $\tilde{\nu}_{\text{CO}} = 2038, 1959, 1907\text{cm}^{-1}$; elemental analysis calcd (%) for $\text{C}_{124}\text{H}_{80}\text{O}_{12}\text{P}_8\text{Cl}_4\text{Re}_4$ (2896.35): C 51.42, H 2.78; found C 51.53, H 2.95.

Synthesis of $[\text{Os}(\text{bpy})_2(\text{C}_2\text{P}_2)_2](\text{PF}_6)_2$ (5**):** A suspension of $[\text{Os}(\text{bpy})_2(\text{CO}_3)]$ and C_2P_2 (1:2.5 ratio) in ethylene glycol/THF (30 mL, 1:2 v/v) was refluxed for 2 h. An excess amount of NH_4PF_6 (200–300 mg) was then added, and the mixture was refluxed for an additional 48 h. The solution was cooled down to room temperature. THF was removed, and the remaining solution in ethylene glycol was added dropwise to a saturated solution of KPF_6 in H_2O (60 mL). The precipitate thus formed was collected by vacuum filtration, washed with H_2O (3×10 mL) and diethyl ether (3×10 mL), and then dried in vacuo. The brown product was purified by basic alumina column chromatography using a CH_3CN /toluene mixture (1:2 v/v) as eluant. The desired product was isolated as the first portion (yield 30 %). The second portion was identified as the bimetallic side product.

$^{31}\text{P}\{^1\text{H}\}$ NMR (202 MHz, CD_3CN , 25 °C): $\delta = -9.8$ (s, $\text{Os}^{\text{II}}-\text{PPh}_2$), -30.9 (s, free PPh_2); FAB/MS: (m/z): 1436 $[\text{M} - \text{PF}_6]^+$, 1289 $[\text{M} - 2\text{PF}_6]^+$; ESI/MS: (m/z): 14370 $[\text{M} - \text{PF}_6]^+$, 645.5 $[\text{M} - 2\text{PF}_6]^{2+}$; elemental analysis calcd (%) for $\text{C}_{72}\text{H}_{58}\text{ON}_4\text{P}_6\text{F}_{12}\text{Os}$ (1599.29): C 54.07, H 3.66; found C 54.53, H 3.25.

Synthesis of heterometallic $[\{\text{Re}(\text{CO})_5\text{Cl}_2(\text{Os}(\text{bpy})_2)_2(\text{C}_2\text{P}_2)_4](\text{PF}_6)_4$ (6**):** A solution of $[\text{Re}(\text{CO})_5\text{Cl}]$ and **5** (1:1 ratio) in ethylene glycol/THF (100 mL, 1:9 v/v) was refluxed for three days. The solution was then cooled down to room temperature. THF was removed, and the residue was added dropwise to a saturated solution of KPF_6 in H_2O (60 mL). The brown precipitate was collected by vacuum filtration, washed with H_2O (3×10 mL) and diethyl ether (3×10 mL), and then dried in vacuo. The product was then purified by basic alumina column chromatography using acetonitrile and methanol as eluants. The desired product was isolated as the second portion using methanol eluant (yield 25 %).

$^{31}\text{P}\{^1\text{H}\}$ NMR (202 MHz, CD_3CN , 25 °C): $\delta = -8.3$ (s, $\text{Re}-\text{P}$), -9.1 (s, $\text{Os}-\text{P}$); FAB/MS: (m/z): 3354 $[\text{M} - 3\text{PF}_6 + \text{O}]^+$, 2479 $[\text{M} - \text{Re}(\text{CO})_5\text{Cl}(\text{C}_2\text{P}_2)_2 - 2\text{CO} - \text{PF}_6]^+$; ESI/MS: (m/z): 1650.5 $[\text{M} - 3\text{PF}_6 - \text{Cl}]^{2+}$, 1051.7 $[\text{M} - 4\text{PF}_6 - \text{Cl}]^{3+}$; FT-IR: $\tilde{\nu}_{\text{CO}} = 2037, 1965, 1918\text{cm}^{-1}$; elemental analysis calcd (%) for $\text{C}_{150}\text{H}_{120}\text{O}_{10}\text{N}_8\text{Cl}_2\text{P}_{12}\text{F}_{24}\text{Re}_2\text{Os}_2$ (3845.96): C 46.85, H 3.29; found C 46.35, H 3.15.

X-ray structure determination: A colorless crystal of $[\{\text{Re}(\text{CO})_5\text{Cl}(\text{C}_2\text{P}_2)\}_2]$ with dimensions $0.07 \times 0.10 \times 0.30$ mm was mounted on a glass fiber and transferred to a Siemens CCD platform diffractometer. The SMART program package^[22a] was used to determine the unit-cell parameters and for data collection (30 sec/frame scan time for a hemisphere of data). The raw frame was processed using SAINT^[22b] and SADABS^[22c] to yield the reflection data file. Subsequent calculations were carried out using the SHELXTL^[22d] program. The diffraction symmetry was $2/m$, and the systematic absences were consistent with the centrosymmetric monoclinic space group $P2_1/n$; this was later determined to be correct.

The structure was solved by direct methods and refined on F^2 by full-matrix least-squares techniques. The analytical scattering factors^[22e] for neutral atoms were used throughout the analysis. The molecule was a dimer and located about an inversion center. There were two molecules of THF solvent present per dimeric formula unit. Hydrogen atoms were located from a difference-Fourier map and refined (x, y, z , and U_{iso}). The hydrogen atoms associated with the THF solvent were included using a refine model. At convergence, $R1 = 0.0316$, $wR2 = 0.0496$, and $\text{GOF} = 1.036$ for 451 variables refined against 7171 unique data. As a comparison for refinement on F , $R1 = 0.0226$ and $wR2 = 0.0472$ were obtained for those 6127 data with $I > 2.0\sigma(I)$. Crystallographic data and data collection parameters are provided in Table 1. Selected bond lengths and bond angles are given in Table 2.

Crystallographic data (excluding structure factors) for the structure (**1**) reported in this paper have been deposited with the Cambridge Crystallographic Data Centre as supplementary publication no. CCDC-149655. Copies of the data can be obtained free of charge on application to CCDC, 12 Union Road, Cambridge CB21EZ, UK (fax: (+44)1223-336-033; e-mail: deposit@ccdc.cam.ac.uk).

Acknowledgements

This work was supported by the University of California, Irvine and NSF-CAREER award (CHE-9733546). We thank Dr. John Greaves (UCI Mass Spectral Facility) for his help in the measurement of FAB/MS and ESI/MS data. We also acknowledge the Beckman Laser Institute in Irvine, CA for the use of the SLM-Aminco 48000 MHF Fourier Transform Spectrofluorometer to measure the lifetimes.

- [1] For representative recent review articles, see: a) S. Leininger, B. Olenyuk, P. J. Stang, *Chem. Rev.* **2000**, *100*, 853–908; b) M. Fujita, *Acc. Chem. Res.* **1999**, *32*, 53–61; c) D. L. Caulder, K. N. Raymond, *Acc. Chem. Res.* **1999**, *32*, 975–982; d) R. V. Slone, K. D. Benkstein, S. Bélanger, J. T. Hupp, I. A. Guzei, A. L. Rheingold, *Coord. Chem. Rev.* **1998**, *171*, 221–243; e) P. J. Stang, B. Olenyuk, *Acc. Chem. Res.* **1997**, *30*, 502–518.
- [2] a) F. A. Cotton, L. M. Daniels, C. Lin, C. A. Murillo, *J. Am. Chem. Soc.* **1999**, *121*, 4538–4539; b) G. R. Newkome, T. J. Cho, C. N. Moorefield, G. R. Baker, R. Cush, P. S. Russo, *Angew. Chem.* **1999**, *111*, 3899–3903; *Angew. Chem. Int. Ed.* **1999**, *38*, 3717–3721; c) E. C. Constable, E. Schofield, *Chem. Commun.* **1998**, 403–404; d) F. S. McQuillan, T. E. Berridge, H. Chen, T. A. Hamer, C. J. Jones, *Inorg. Chem.* **1998**, *37*, 4959–4970; e) P. L. Jones, K. J. Byrom, J. C. Jeffrey, J. A. McCleverty, M. D. Ward, *Chem. Commun.* **1997**, 1361–1362; f) F. M. Remero, R. Ziessel, A. Dupont-Gervais, A. V. Dorsselaer, *Chem. Commun.* **1996**, 551–552; g) E. Solari, W. Lesueur, A. Klöse, K. Schenk, C. Floriani, A. Chiesivilla, C. Rizzoli, *Chem. Commun.* **1996**, 807–808; h) C. M. Drain, J.-M. Lehn, *J. Chem. Soc. Chem. Commun.* **1994**, 2313–2314.
- [3] a) R. V. Slone, D. I. Yoon, R. M. Calhoun, J. T. Hupp, *J. Am. Chem. Soc.* **1995**, *117*, 11813–11814; b) P. D. Beer, F. Szemes, V. Balzani, C. M. Salá, M. G. B. Drew, S. W. Dent, M. Maestri, *J. Am. Chem. Soc.* **1997**, *119*, 11864–11875.
- [4] a) D. Xu, B. Hong, *Angew. Chem.* **2000**, *112*, 1896–1899; *Angew. Chem. Int. Ed.* **2000**, *39*, 1826–1829; b) D. Xu, H. J. Murfee, W. E. van der Veer, B. Hong, *J. Organomet. Chem.* **2000**, *596*, 53–63.
- [5] J.-M. Lehn, *Supramolecular Chemistry*, VCH, New York, **1995**.
- [6] a) S. M. Woessner, J. B. Helms, K. M. Lantzky, B. P. Sullivan, *Inorg. Chem.* **1999**, *38*, 4378–4379; b) S. M. Woessner, J. B. Helms, J. F. Houliis, B. P. Sullivan, *Inorg. Chem.* **1999**, *38*, 4380–4381.
- [7] a) S.-S. Sun, A. J. Lees, *Inorg. Chem.* **1999**, *38*, 4181–4182; b) S.-S. Sun, A. S. Silva, I. M. Brinn, A. J. Lees, *Inorg. Chem.* **2000**, *39*, 1344–1345.
- [8] a) J. V. Caspar, T. J. Meyer, *J. Am. Chem. Soc.* **1983**, *105*, 5583–5590; b) E. M. Kober, J. V. Caspar, B. P. Sullivan, T. J. Meyer, *Inorg. Chem.* **1988**, *27*, 4587–4598; c) E. M. Kober, B. P. Sullivan, W. J. Dressick, J. V. Caspar, T. J. Meyer, *J. Am. Chem. Soc.* **1980**, *102*, 7383–7385; d) S. R. Johnson, T. D. Westmoreland, J. V. Caspar, K. R. Barqawi, T. J. Meyer, *Inorg. Chem.* **1988**, *27*, 3195–3200; e) J. P. Sauvage, J. P. Collin, J. C. Chambron, S. Guillerez, C. Coudret, V. Balzani, F. Barigetti, L. De Cola, L. Flamigni, *Chem. Rev.* **1994**, *94*, 993–1019; f) J. V. Caspar, E. M. Kober, B. P. Sullivan, T. J. Meyer, *J. Am. Chem. Soc.* **1982**, *104*, 630–632.
- [9] a) J. V. Ortega, B. Hong, S. Ghosal, J. C. Hemminger, B. Breedlove, C. P. Kubiak, *Inorg. Chem.* **1999**, *38*, 5102–5112; b) B. Hong, S. V. Woodcock, S. K. Saito, J. V. Ortega, *J. Chem. Soc. Dalton Trans.* **1998**, 2615–2623; c) B. Hong, *Comments Inorg. Chem.* **1999**, *20*, 177–207.
- [10] a) H. J. Murfee, T. P. Thoms, J. Greaves, B. Hong, *Inorg. Chem.* **2000**, *39*, 5209–5217; b) G. Montaudo, M. S. Montaudo, C. Puglisi, F. Samperi, M. Sepulchre, *Macromol. Chem. Phys.* **1996**, *197*, 2615–2625; c) G. Montaudo, M. S. Montaudo, C. Puglisi, F. Samperi, *Rapid Commun. Mass Spectrom.* **1995**, *9*, 453–460; d) H. M. Burger, H. M. Muller, D. Seebach, K. O. Bornsen, M. Schar, H. M. Widmer, *Macromolecules* **1993**, *26*, 4783–4790.
- [11] a) M. N. Ramsis, *Monatsh. Chem.* **1993**, *124*, 849–855; b) K. D. Benkstein, J. T. Hupp, C. L. Stern, *Inorg. Chem.* **1998**, *37*, 5404–5405; c) E. W. Abel, S. P. Tyfield, *Can. J. Chem.* **1969**, *47*, 4627–4633; d) D. A. Edwards, J. Marshalsea, *J. Organomet. Chem.* **1977**, *131*, 73–91; e) J. Huhmann-Vincent, B. L. Scott, G. J. Kubas, *Inorg. Chem.* **1999**, *38*, 115–124.
- [12] a) M. S. Wrighton, D. L. Morse, H. B. Gray, D. K. Ottesen, *J. Am. Chem. Soc.* **1976**, *98*, 1111–1119; b) M. M. Glezen, A. J. Lees, *J. Chem. Soc. Chem. Commun.* **1987**, 1752–1753; c) M. M. Glezen, A. J. Lees, *J. Am. Chem. Soc.* **1988**, *110*, 3892–3897.
- [13] a) P. J. Giordano, M. S. Wrighton, *J. Am. Chem. Soc.* **1979**, *101*, 2888–2889; b) A. J. Lees, *Comments Inorg. Chem.* **1995**, *17*, 319–346; c) J. V. Ortega, K. T. Khin, W. E. van der Veer, J. Ziller, B. Hong, *Inorg. Chem.* **2000**, *39*, 6038–6050; d) K. D. Ley, K. S. Schanze, *Coord. Chem. Rev.* **1998**, *171*, 287–307.
- [14] a) V. Balzani, S. Campagna, G. Denti, A. Juris, S. Serroni, M. Venturi, *Acc. Chem. Res.* **1998**, *31*, 26–34; b) G. D. Storrier, K. Takada, H. D. Abruña, *Langmuir* **1999**, *15*, 872–884.
- [15] a) B. P. Sullivan, D. J. Salmon, T. J. Meyer, *Inorg. Chem.* **1978**, *17*, 3334–3341; b) P.-W. Wang, M. A. Fox, *Inorg. Chem.* **1995**, *34*, 36–41.
- [16] a) R. Englman, J. Jortner, *Mol. Phys.* **1970**, *18*, 145–164; b) K. Freed, J. Jortner, *J. Chem. Phys.* **1970**, *52*, 6272–6291.
- [17] a) N. S. Hush, *Prog. Inorg. Chem.* **1967**, *8*, 391–444; b) N. S. Hush, *Electrochim. Acta* **1968**, *13*, 1005; c) C. R. Bock, J. A. Connor, A. R. Gutierrez, T. J. Meyer, D. G. Whitten, B. P. Sullivan, J. K. Nagle, *J. Am. Chem. Soc.* **1979**, *101*, 4815–4824.
- [18] B. J. Pantuch, D. E. Lacky, G. A. Crosby, *J. Phys. Chem.* **1980**, *84*, 2061–2067.
- [19] a) F. Barigelletti, L. Flamigni, V. Balzani, J.-P. Colin, J.-P. Sauvage, A. Sour, E. C. Constable, A. M. W. C. Thompson, *J. Am. Chem. Soc.* **1994**, *116*, 7692–7699; b) V. Balzani, A. Juris, M. Venturi, S. Campagna, S. Serroni, *Chem. Rev.* **1996**, *96*, 759–833; c) L. De Cola, V. Balzani, F. Barigelletti, L. Flamigni, P. Belser, A. von Zelewsky, M. Frank, F. Vögtle, *Inorg. Chem.* **1993**, *32*, 5228–5238.
- [20] a) V. Grosshenny, A. Harriman, F. M. Romero, R. Ziessel, *J. Phys. Chem.* **1996**, *100*, 17472–17484; b) A. Harriman, R. Ziessel, *Chem. Commun.* **1996**, 1707–1716.
- [21] C. A. Parker, W. T. Rees, *Analyst (London)* **1960**, *85*, 587–600.
- [22] a) *SMART Software Users Guide Version 4.21*, Bruker Analytical X-ray Systems, Inc. Madison, WI, **1997**; b) *SAINT Software Users Guide Version 4.05*, Bruker Analytical X-ray Systems, Inc. Madison, WI, **1997**; c) G. M. Sheldrick, *SADABS*, Bruker Analytical X-ray Systems, Inc.; Madison, WI, **1997**; d) G. M. Sheldrick, *SHELXTL Version 5.10*, Bruker Analytical X-ray Systems, Inc. Madison, WI, **1997**; e) *International Tables for X-ray Crystallography Vol. C* Dordrecht, Kluwer, **1992**.

Received: September 27, 2000 [F2758]